Published in IET Microwaves, Antennas & Propagation
Received on 20th January 2010
Revised on 27th May 2010
doi: 10.1049/iet-map.2010.0024

ISSN 1751-8725

# Constitutive parameter extraction and experimental validation of single and double negative metamaterials

*Y. Hollander*[1] *R. Shavit*[2]

[1]*Department of Electro-Optical Engineering, Ben-Gurion University of the Negev, Beer Sheva 84105, Israel*
[2]*Department of Electrical and Computer Engineering, Ben-Gurion University of the Negev, Beer Sheva 84105, Israel*
*E-mail: rshavit@ee.bgu.ac.il*

**Abstract:** In this study, two independent methods to extract the constitutive parameters of large-scale (more than a wavelength long) metamaterial (MTM) structures are described. One method is based on fitting the simulated inner electric/magnetic field to the electric/magnetic field computed with an analytical model, whereas the other method is based on the scattering matrix parameters. The extraction methods are tested on three MTM structures [two single negative and one double negative (DNG)] and show results that are in good agreement. The extracted parameters were used to predict a focusing effect in a simulated spherical concave lens made of DNG MTM. The three MTM structures were experimentally measured for insertion loss in an anechoic chamber. For practical reasons, the experimental models were fabricated on Duroid substrates and scaled to operate in X-band. Detailed explanation of the construction of the MTMs and the anechoic chamber measurement setup is given. The transmission characteristics were measured at different frequencies and at different incident angles. The measured and simulated results are found to be in good agreement. In the DNG MTM, a peak transmission of −0.7 dB was measured, which to these authors' knowledge is the highest reported to date for such an MTM structure. Good transmission is maintained for incident angles of up to 45° from boresight.

## 1 Introduction

The relative electrical permittivity, $\varepsilon_r$, and relative magnetic permeability, $\mu_r$, are the constitutive parameters, which determine the propagation of electromagnetic (EM) waves in matter. The propagation constant, $k$, in an isotropic material is equal to $(\omega/c)\sqrt{\mu_r\varepsilon_r} = (\omega/c)n$, in which $n = \sqrt{\varepsilon_r\mu_r}$ is the refractive index, $\omega$, is the angular frequency and $c$ is the free space speed of light. Mathematically and physically, a material can have permeability and permittivity parameters as double positive (DPS), double negative (DNG) or single negative (SNG) [1]. Within an SNG material and for frequencies below the plasma frequency, the EM theory predicts the existence of evanescent modes, thus having exponentially decaying fields as a function of distance inside the material. In contrast, in a DNG material the fields propagate and exhibit some unusual phenomena. Perhaps the most interesting of these is negative refraction [1]. SNG and DNG metamaterials (MTMs) have become feasible in the last decade. The most common MTM to achieve this unique characteristic is composed of periodic grids of wires [2] and/or split ring resonators (SRRs) [3]. Extractions of the effective constitutive parameters of these complex structures have been done most commonly using the scattering matrix technique as reported in [4–6]. This technique relies on the MTM thickness to be as small as possible in order to avoid ambiguity in the determination of the correct branch when calculating the refractive index. However, this runs in contradiction with the findings that homogenisation of MTMs is accurate only on large-scale models and that the extracted parameters of the MTMs are dependent on the physical size of the structures [7–9].

In this paper, it is demonstrated that for a large-scale (along the propagation axis) MTM structure, it is possible to extract the constitutive parameters by utilising a

modification to the scattering matrix technique, which avoids this ambiguity. This approach is validated by using finite-element simulations in the 5–6.5 GHz frequency range in order to reproduce results presented in [10]. The results are validated by comparison to a second technique called the 'fields' method in which the MTM's inner electric/magnetic field amplitude/phase is compared to the fields of an analytic model having constitutive parameters of similar values. The importance of analysing a large-scale structure (larger than a wavelength) implies that parameter retrieval based on a single unit cell is not as accurate. This observation was also confirmed in the current paper. Analysis of a large-scale MTM structure is also essential for gaining a better physical understanding of the nature of the MTMs. Inspection of the amplitude and phase of the fields inside the structure is utilised as well with the fields method. In this study, it has also been recognised that the physical size of the structure to be taken for the S-parameter reference planes is not identical to the physical size of the structure but coincides with the first and last edges of the SRR elements. The two extraction methods (scattering matrix technique and the fields method) considered in this work show good agreement. Additional validation of the DNG extracted parameters was performed by simulating an MTM spherical concave lens made entirely of wires and SRRs. The same contoured lens made of DPS material produces a divergent lens but, when composed of wires and SRRs that form a DNG material, produces a focusing lens with a focal length that agrees with the same DNG constitutive parameters as extracted earlier from the DNG MTM. Owing to practical considerations of realisation and availability of measurement antennas and testing equipment, the MTMs (two SNGs and one DNG) were scaled to X-band. The geometry in the X-band was simulated, fabricated and tested in an anechoic chamber for insertion loss at different frequencies and different incident angles. The results show, as expected, poor transmittance for the two SNG materials and good transmittance for the DNG material. The agreement between simulation and the experimental results is good.

## 2 Field behaviour inside a SNG slab and the resulting fields extraction method

The normalised field amplitude along the propagation axis for a normally incident plane wave inside a homogenous SNG slab with finite thickness can be expressed by

$$E(d) = \mathrm{e}^{-k_0 d\sqrt{|\mu_\mathrm{r}|}\sqrt{|\varepsilon_\mathrm{r}|}} + \Gamma_2 \mathrm{e}^{k_0 d\sqrt{|\mu_\mathrm{r}|}\sqrt{|\varepsilon_\mathrm{r}|}} \quad (1)$$

in which $d$ is the location along the field propagation axis in the slab starting at the first (incident) interface and $\Gamma_2$ is the reflection coefficient from the second interface of the slab which can be expressed as [11]

$$\Gamma_2 = \left[\frac{1-\sqrt{(\mu_\mathrm{r}/\varepsilon_\mathrm{r})}}{1+\sqrt{(\mu_\mathrm{r}/\varepsilon_\mathrm{r})}}\right] \mathrm{e}^{-2k_0 d\sqrt{|\mu_\mathrm{r}||\varepsilon_\mathrm{r}|}} \quad (2)$$

It is evident that the thicker the SNG slab is, the less significant the second term on the right-hand side of (1) becomes, and (1) resembles more an evanescent mode inside a semi-infinite SNG medium. We conclude that for large-scale SNG structures, omitting the second term of (1) has negligible impact on the total field inside the material yielding

$$E(d) = \mathrm{e}^{-k_0 d\sqrt{|\mu_\mathrm{r}|}\sqrt{|\varepsilon_\mathrm{r}|}} \quad (3)$$

which predicts an exponentially decaying electric field (evanescent mode). Based on (3), and assuming negative permittivity and positive permeability, $\varepsilon_\mathrm{r}$ can be computed through

$$|\varepsilon_\mathrm{r}| = \left[\frac{\ln E(d)}{k_0 d|\mu_\mathrm{r}|}\right]^2 \quad (4)$$

Similarly, assuming negative permeability and positive permittivity, $\mu_\mathrm{r}$ can be computed through

$$|\mu_\mathrm{r}| = \left[\frac{\ln H(d)}{k_0 d|\varepsilon_\mathrm{r}|}\right]^2 \quad (5)$$

Although $\varepsilon_\mathrm{r}$ and $\mu_\mathrm{r}$ are positive in (4) and (5), respectively, it must be remembered that the initial expression (3) used to derive them is based on the assumption that the slab is SNG or in other words $\varepsilon_\mathrm{r} < 0$ ($\mu_\mathrm{r} > 0$) or $\mu_\mathrm{r} < 0$ ($\varepsilon_\mathrm{r} > 0$). This permits the addition of a negative sign to the final values of (4) and (5). The above extraction technique is termed the fields method hereon.

## 3 Simulation and extraction of the constitutive parameters of SNG MTMs

### 3.1 Structure and simulation description

Two SNG MTM structures are considered for the analysis: one wire-based and the other SRR-based. The simulations have been performed with the commercial EM software, Microwave Studio from CST, and are based on its frequency domain solver. The simulated structures do not include dielectric substrates to avoid secondary parasitic effects. Figs. 1 and 2 show the two SNG MTMs (wire-based and SRR-based), which in general resemble the structure in [10] but with several modifications: the wires are infinitely long instead of finite (in the $x$-axis), the SRRs are rotated 90° so that their air gaps are symmetric in relation to the incident electric field wave and there are nine unit cells along the propagation axis which totals the MTM structures' thickness

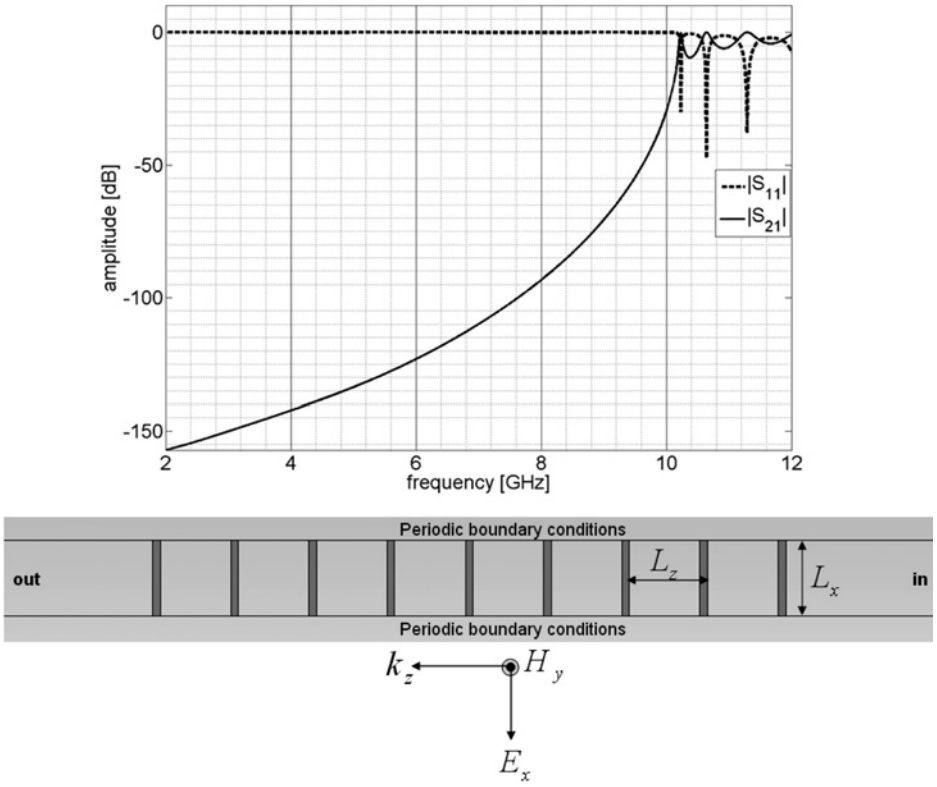


**Figure 1** *Wire-based large-scale MTM simulated geometry*
Inset shows its reflection and transmission characteristics

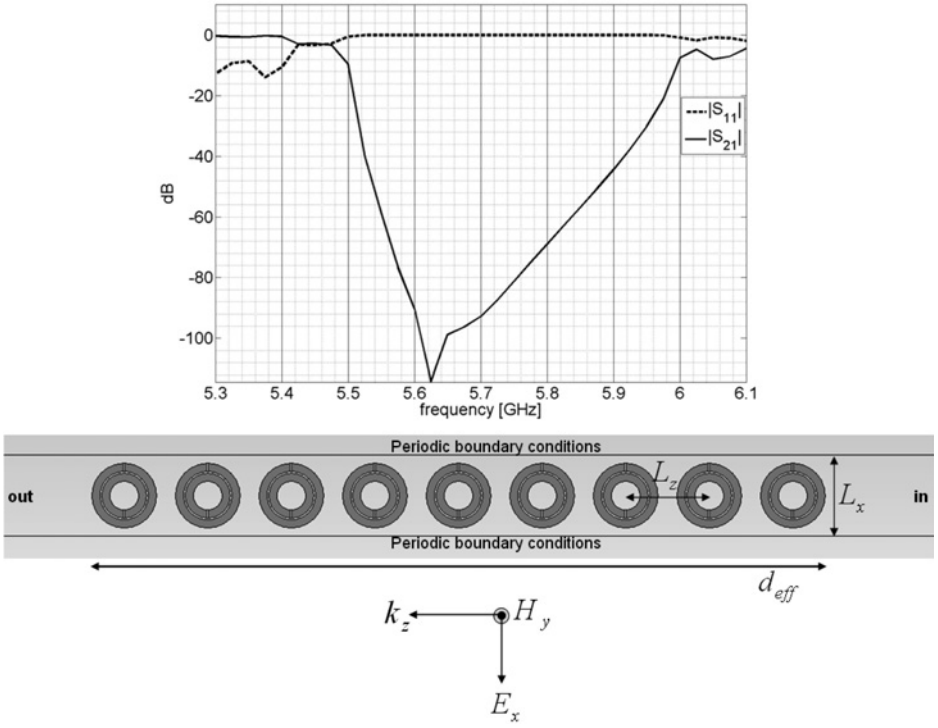


**Figure 2** *SRR-based large-scale MTM simulated geometry*
Inset shows its reflection and transmission characteristics

at ~1.5 wavelengths. The structures have periodicities along $z$- and $x$-axis of $L_z = 9.3$ mm and $L_x = 9$ mm, respectively. Along the $y$-axis the periodicity is 6.5 mm. The width of the wires and SRRs is 0.9 mm and the SRR air gaps are 0.2 mm wide. The outer and inner SRR central radii are equal to 3.6 and 1.6 mm, respectively. Periodic boundary



doi: 10.1049/iet-map.2010.0024

conditions are placed at the edges of the geometry on the $x$- and $y$-axis in order to simulate infinitely periodic structures. An $x$-polarised electric field is incident on the structure from right to left at normal incidence. The frequency of interest is 5–6 GHz.

## 3.2 Extraction of the constitutive parameters

The amplitudes of the complex transmission coefficient, $S_{21}$, and the complex reflection coefficient, $S_{11}$, obtained from simulations on the wire MTM are shown in the inset of Fig. 1. Total reflection is seen in the desired frequency range. The continuous line in Fig. 3 describes the normalised electric field amplitude along the propagation axis for a sample frequency of 5.8 GHz as simulated by CST. It gives an insight to the evanescent trend of the fields in the MTM. The ripple is caused by the strong interactions between the incident electric field and the wires. The dashed line of Fig. 3 shows the computed analytic electric field using (3) for a homogenous slab with the same length, $d_{\text{eff}}$, as the actual structure making the assumption that $\mu_r = 1$ (no magnetic attributes are assumed for the wires). This assumption points to a certain limitation of the method, which is the requirement of a priori knowledge of the permeability in case of MTM with negative permittivity and a priori knowledge of the permittivity in case of MTM with negative permeability. Variation of the permittivity or permeability values in the homogeneous slab to match the field amplitude function of the actual structure (wires only or SRRs only) results in the effective permittivity or permeability of the SNG structures. Note that this field trend fitting is possible only for large-scale structures. One unit cell does not have sufficient effective material width to view properly the field trend. This technique has been repeated for several other frequencies and the results are shown in Fig. 4 labelled by 'fields method'. In order to verify these results, another extraction method, namely the 'S-parameter method' described in [4–6] has been applied. This method allows

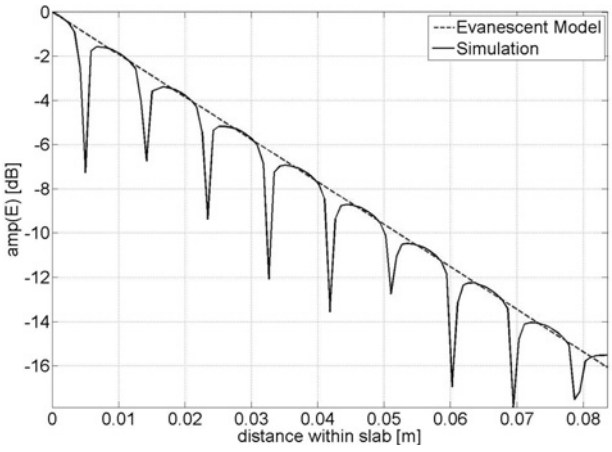


**Figure 3** *Normalised simulated electric field amplitude compared to the evanescent model*

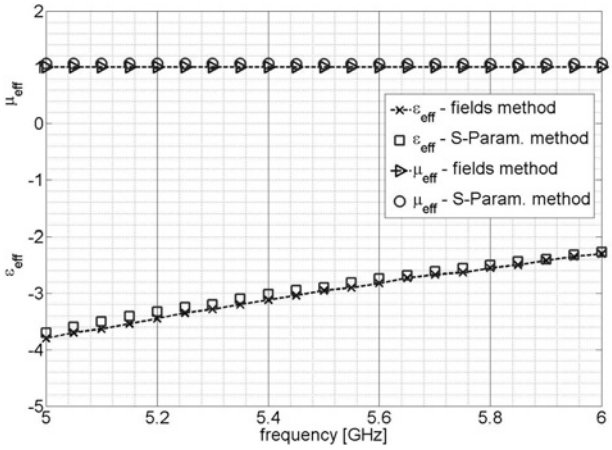


**Figure 4** *Comparison between the effective permittivity, $\varepsilon_{eff}$, and permeability, $\mu_{eff}$, of the wire structure computed with the fields method and the S-parameter method*

the extraction without ambiguity of the constitutive parameters in very short (in wavelengths) MTM structures. As discussed before, it is important to analyse large-scale structures as opposed to single unit cells. Utilising some of the advantages found in CST can help in resolving the ambiguities of a large-scale structure, as well as give important physical insight into the nature of the structures. The techniques for resolving the ambiguities are outlined in [12] and repeated here for convenience:

1. The wavelength within the structure, $\lambda_g$, can be obtained via simulation and thus determine the refraction index: $n = \sqrt{\mu_r \varepsilon_r} = \lambda_0/\lambda_g$. This technique is helpful in DNG analysis.

2. Simulations of different slab thicknesses must result in the same effective permittivity and permeability. This technique applies for both SNG and DNG analyses.

3. In simulations of lossless materials (no loss in dielectric and the elements are made of perfect electric conductor (PEC) only one branch of $\varepsilon_r$ and $\mu_r$ will result in an imaginary part equal to zero. This technique applies for both SNG and DNG analyses.

The retrieved parameters of the wire structure of Fig. 1, using the 'S-parameter' method assisted by the above techniques for ambiguity elimination, are shown in Fig. 4 and appear to be in good agreement with the fields method results. It is clear that the assumption of the permeability being equal to 1 in the fields method is a good assumption and in fact within 3% of the actual ~1.03 value determined by the S-parameter method.

Next, an MTM based on SRRs, as shown in Fig. 2, was simulated using the same procedure outlined above. The amplitudes of the transmission and reflection coefficients are shown in the inset of Fig. 2. Total reflection is visible

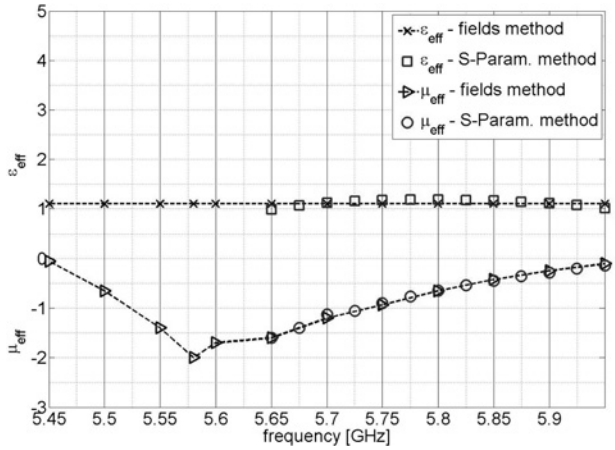


**Figure 5** *Comparison between the effective permittivity, $\varepsilon_{eff}$, and permeability, $\mu_{eff}$, of the SRR structure computed with the fields method and the S-parameter method*

from 5.45 to 5.90 GHz. In order to calculate the effective permeability with the fields method, the effective permittivity value for the structure is a priori required as prescribed by (5). This value has been analytically calculated in [3] and reproduced here

$$\varepsilon_{\text{eff}} = \left(1 - \frac{\pi r^2}{L_z^2}\right)^{-1} \tag{6}$$

in which $r$ is the inner central radius of the SRRs and is equal to 1.6 mm. Calculation of (6) gives a permittivity value of 1.1. The computed inner fields of this structure resemble very much that in Fig. 3 and differ mainly in amplitude. In accordance with the fields method, variation of the permeability value in the homogeneous slab to match the field amplitude function of the SRR SNG structure, results in the effective permeability. Comparison of the results with the extracted effective parameters calculated using the S-parameter method is summarised in Fig. 5. Good agreement is seen between the results obtained by the two methods. Note that the S-parameter method results at 5.45–5.60 GHz are not shown owing to an erratic behaviour of the S-parameter-simulated phases. This is believed to be caused by the strong resonance occurring near 5.45 GHz, which may require even finer meshing of the SRR elements at these frequencies. Nonetheless, the SNG nature of the SRR MTM is observed and good agreement of the extracted parameters between the two methods is clearly seen.

## 4 Simulation, extraction and validation of the constitutive parameters of a DNG MTM

Once the SNG attributes in the required frequency range have been computed, the two SNG MTMs are combined together as shown in Fig. 6 in order to obtain DNG attributes. The

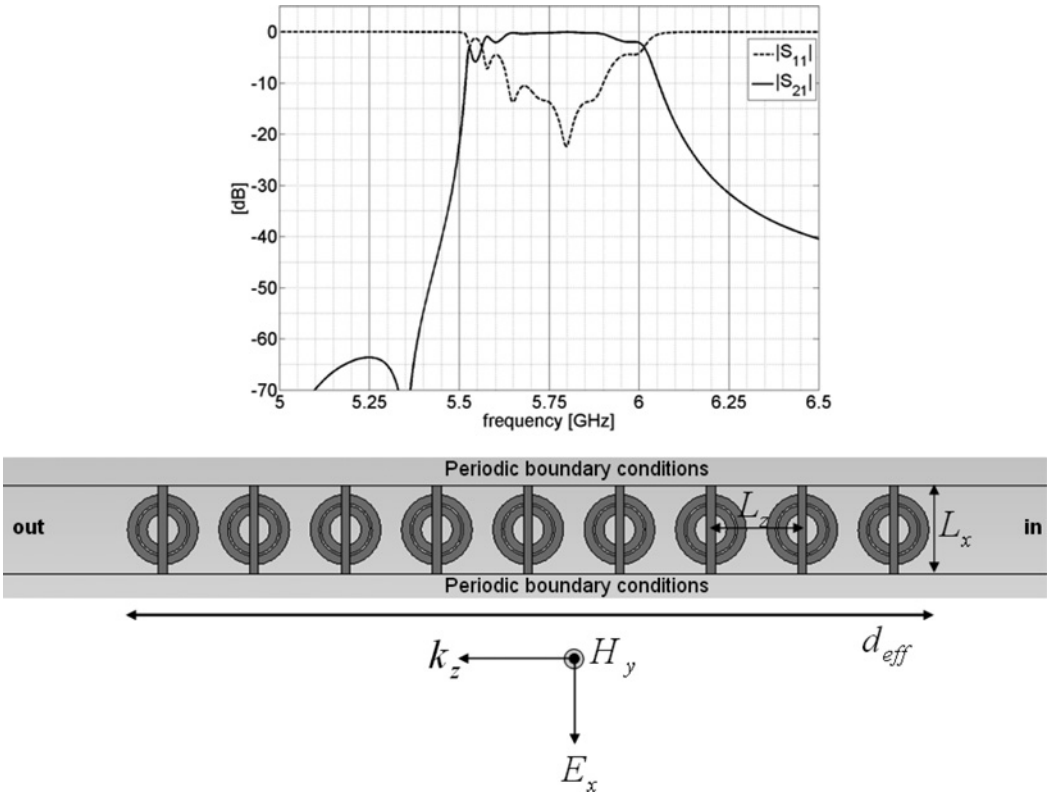


**Figure 6** *Combined wires and SRRs MTM simulated geometry*
Inset shows the computed reflection and transmission characteristics




doi: 10.1049/iet-map.2010.0024

**Table 1** Extracted permittivity and permeability values of the DNG MTM

| Frequency, GHz | $\varepsilon_r$ DNG | $\mu_r$ DNG |
|---|---|---|
| 5.65 | −2.2 | −1.14 |
| 5.70 | −0.7 | −2.93 |
| 5.75 | −0.91 | −1.61 |
| 5.80 | −0.8 | −1.16 |
| 5.85 | −0.92 | −0.8 |
| 5.90 | −0.93 | −0.6 |
| 5.95 | −1.6 | −0.24 |

spacing in the $y$-direction between the SRRs and the wires is set to 1.5 mm. The inset of Fig. 6 shows the transmission and reflection characteristics of the newly created structure. Clearly, now the new combined structure is showing very good transmission characteristics in the frequency range in which each SNG structure had previously resulted in total reflection. This is a good indication that the new structure combined from the two SNG structures results in a DNG MTM. Application of the S-parameter method to the new structure results in negative permittivities and negative permeabilities as shown in Table 1.

In order to avoid ambiguity in the retrieval process, use has been made with the procedure outlined in Section 3.2, and more precisely with techniques 1 and 2.

The extracted permittivity and permeability values obtained with the S-parameter method were used to compute the electric field phase in a homogenised DNG slab and have been compared with the simulated electric field phase of the actual structure as computed by simulation. The comparison is shown in Fig. 7. One can observe the phase slope reversal inside the MTM in accordance with theory of DNG materials. Moreover, the effective thickness of the DNG MTM slab structure was found to be 2.5 mm shorter than that of the physical thickness composed of nine unit cells of 9.3 mm or a total of 83.7 mm. This observation has been concluded based on the optimisation of matching between the electric field phases for the homogenous against simulated cases as seen in Fig. 7. This result is in accordance with [5], which has also concluded that the scattering parameters' planes of reference coincide with the first and last unit-cell boundaries of the SRRs.

## 4.1 Validation of DNG extracted parameters by lens simulation

In order to observe the negative refraction effect and validate the extracted parameters of the DNG MTM, half of a spherical concave lens made entirely of wires and SRRs was studied by means of simulation. The geometry is shown in Fig. 8, with the wires and SRRs being the same as in Fig. 6. The lens is bounded at the bottom by PEC boundary conditions which complement the half lens geometry into a full lens simulation. A focal point emerges at 60 mm away from the centre of the lens. The lens is flat on one side ($R_1 = \infty$) and spherical on the other side, with a radius of curvature $R_2 = 118.5$ mm. In the $y$-direction the lens is infinite, as was the case in previous simulations. For DPS materials, this type of lens is diverging (waves would refract upwards in Fig. 8) for a plane wave incident

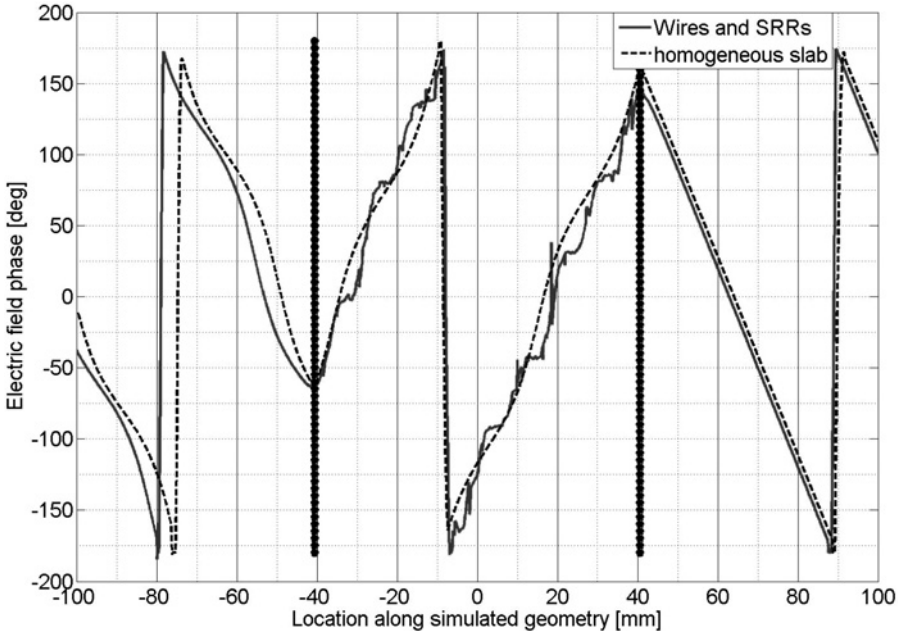


**Figure 7** *Comparison between the electric field phase at 5.8 GHz in the combined wires and SRR structures and in the homogenous slab with the extracted constitutive parameters*

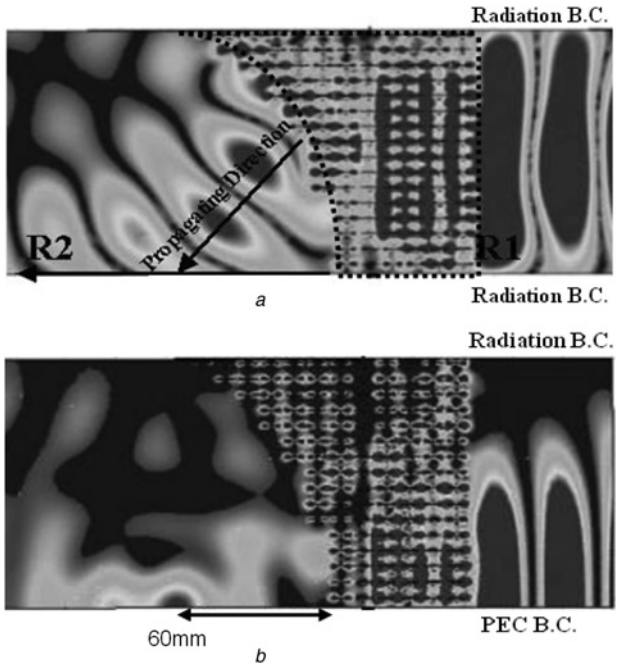


**Figure 8** *Simulation of a DNG structure made of wires and SRRs formed in the shape of a DPS half diverging lens at 5.8 GHz*

*a* Spatial electric field intensity with radiation boundary condition at the bottom

*b* PEC boundary conditions complement the half lens geometry into a full lens simulation. A focal point emerges at 60 mm away from the lens centre

from the right. However, since for a DNG material the refraction index is negative, the waves refract in the opposite direction (downwards) and thus the lens turns into a focusing lens. To demonstrate the negative refraction effect, the simulated structure was illuminated by a plane wave incident from the right at an operating frequency of 5.8 GHz, as shown in Fig. 8. Based on the electric field intensity map in the lens and its vicinity, one can observe the negative refraction effect in accordance to the expected behaviour of a DNG MTM. Using the extracted permittivity and permeability of the DNG MTM at 5.8 GHz as outlined in Table 1, the refractive index, $n$, is equal to $n = 0.93$. In this case the geometrical optics predicts a focal length of 61.4 mm [13]

$$\frac{1}{f} = (n-1)\left(\frac{1}{R_1} - \frac{1}{R_2}\right) \tag{7}$$

in which $f$ is the focal length, and $R_1$, $R_2$ are the first and second curvature lens radii as encountered by the incident wave. The simulation was repeated and a clearly visible focal point emerged. The focal length of the MTM lens is seen in Fig. 8. Measurement of the distance from the centre of the spherical part of the lens to the visible focal point in the electric field intensity map reveals a focal length of ~60 mm, which is very close (within simulation

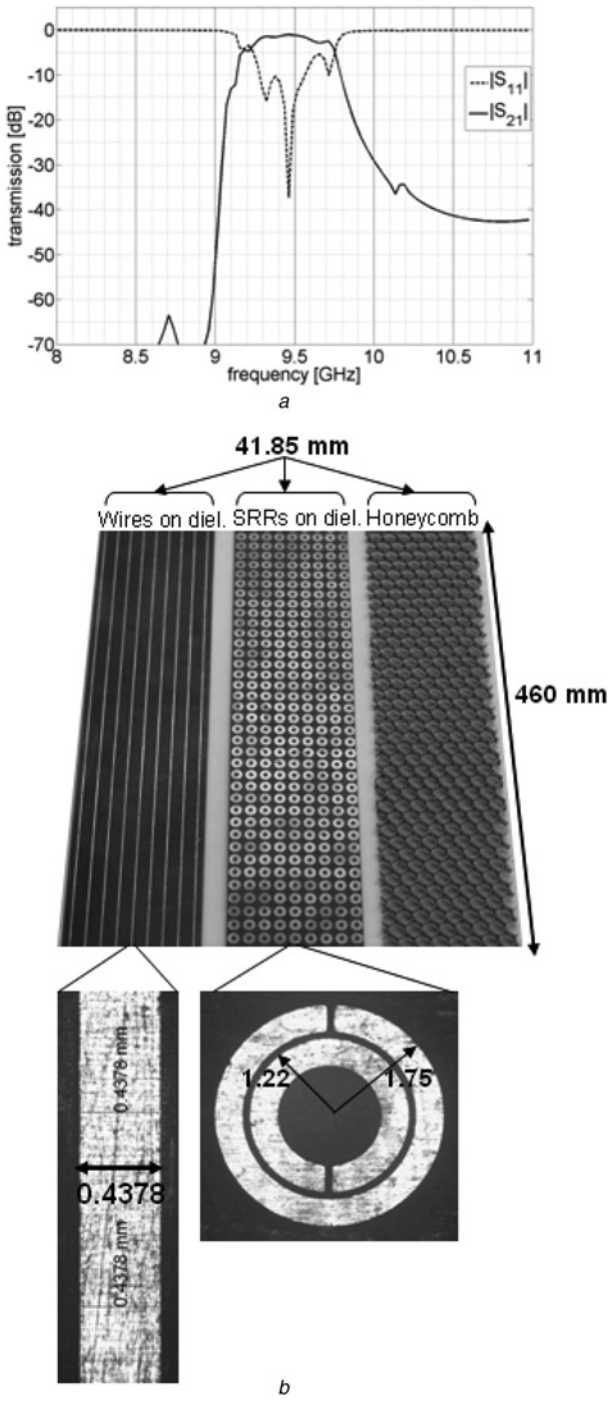


**Figure 9** *Experimental model structure and its simulated electrical performance*

*a* Simulated frequency response (transmission and reflection) of the realised MTM made up of wires, SRRs and honeycomb at X-band

*b* Front side of a dielectric sheet printed with wires and back side of the dielectric sheet printed with SRRs. All sizes are in millimetres

and parameters extraction errors) to the theoretically calculated 61.4 mm from (7).

These findings further ascertain that the simulated MTM structure indeed exhibits a DNG nature and certifies the




doi: 10.1049/iet-map.2010.0024

constitutive parameter extraction process along with the proposed techniques for overcoming the procedure ambiguity.

## 5 Experimental results

In order to test and validate experimentally the SNG and DNG MTM constitutive parameter extraction procedure, three prototypes were built. One made of wires to simulate negative permittivity, one made of SRRs to simulate negative permeability and one combined of wires and SRRs to simulate negative permittivity and permeability simultaneously. The models are made of stacked dielectric substrates separated by honeycomb sheets. For practical reasons of available measurement equipment and improve the accuracy of the transmission measurements through the printed dielectrics, it has been decided that all prototypes will be designed, fabricated and measured in X-band. Accordingly, all physical dimensions were scaled to fit the new frequency band. The unit cell physical dimensions of the three X-band periodic MTM structures are $L_x = 4.5$ mm, $L_y = 4.0$ mm and $L_z = 4.65$ mm. The width of the wires and SRRs is 0.44 mm and the SRR air gaps are 0.1 mm wide. The outer and inner SRR central radii are equal to 1.75 and 1.22 mm, respectively. The wire and SRR elements are made of copper and printed on dielectric substrates from Rogers having electrical parameters $\varepsilon_r = 2.2$, $\tan\ \delta = 0.0009$ and thickness of 0.75 mm. Honeycomb sheets with thickness 3.25 mm separated the dielectric substrates. The overall size of the prototypes was $460 \times 460 \times 41.8\ \text{mm}^3$ with the corresponding number of unit cells $102 \times 115 \times 9$. Fig. 9 shows the components which make the entire model structure and the expected reflection and transmission simulated performance. In the SNG MTM prototypes, the dielectric sheets are printed single-sided with either SRRs or wires, and honeycomb sheets are used for separation. In the DNG MTM prototype, the dielectric sheets are printed on both sides (wires on one side and SRRs on the opposite side) with honeycomb sheets used for separation. The overall dimensions of the SNG MTM prototypes are identical to those of the DNG MTM prototype. Verification of the etching process was accomplished by using a microscope to measure the SRR radii, copper width etc. A sample of a microscope picture is shown in Fig. 9. A computer EM simulation of the DNG MTM experimental structure has shown that the working frequency band is 9.2 − 9.75 GHz.

The complete measurement setup is shown in Fig. 10. The experimental setup inside the anechoic chamber consists of two horizontal ($x$-axis oriented) linear polarised transmitting and receiving antennas located at far-field distance. The MTM prototype was rotated in front of the transmitting antenna. Measurements were performed between 7 and 18 GHz at incident angles ranging from $-45$ to $+45^\circ$ with respect to the normal of the prototype. Within this rotation angular sector, the transmission characteristics through the prototype can be measured with only minor edge diffraction interference. An HP 8530 network analyser was used to collect the received data. Comparison between experimental and simulations results at normal incidence for all three prototypes is shown in Fig. 11. Good agreement can be noticed for all three structures within the dynamic range that can be achieved based on our experimental instrumentation/facilities, which can differentiate between noise and actual data at levels as low as approximately $-45$ dB (better dynamic range may be very difficult to achieve because of RF leakage into the available anechoic chamber at these frequencies).

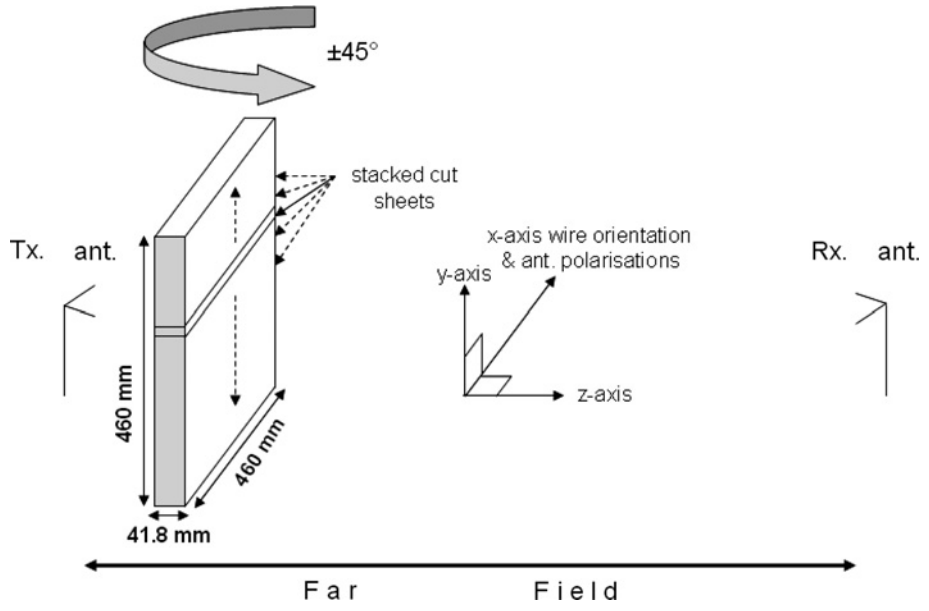


**Figure 10** *Anechoic chamber measurement setup*

Antennas are polarised along the $x$-axis whereas propagation takes place along the $z$-axis

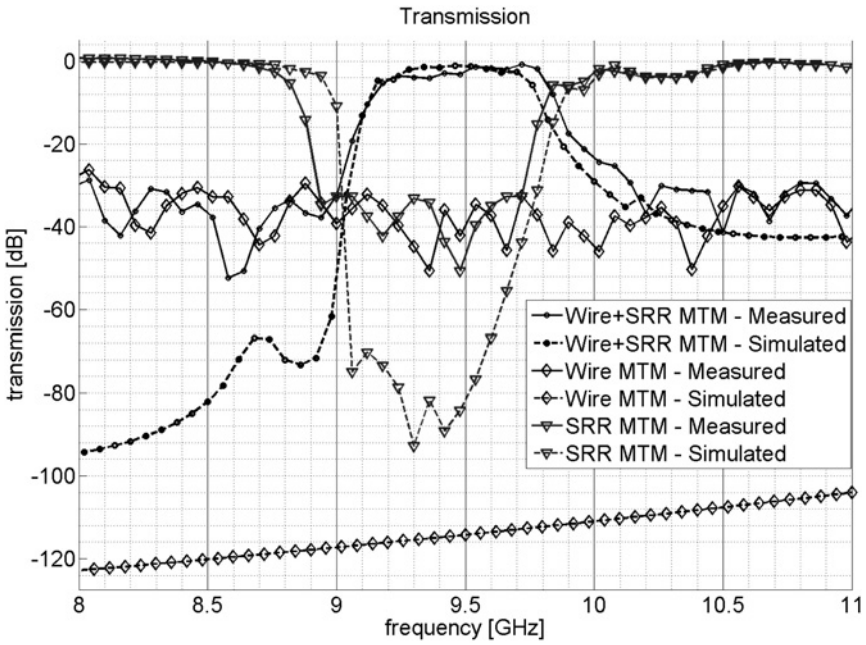


**Figure 11** *Transmission loss simulations and measured results of three structures: wire MTM, SRR MTM, and combined wires and SRRs at normal incidence*

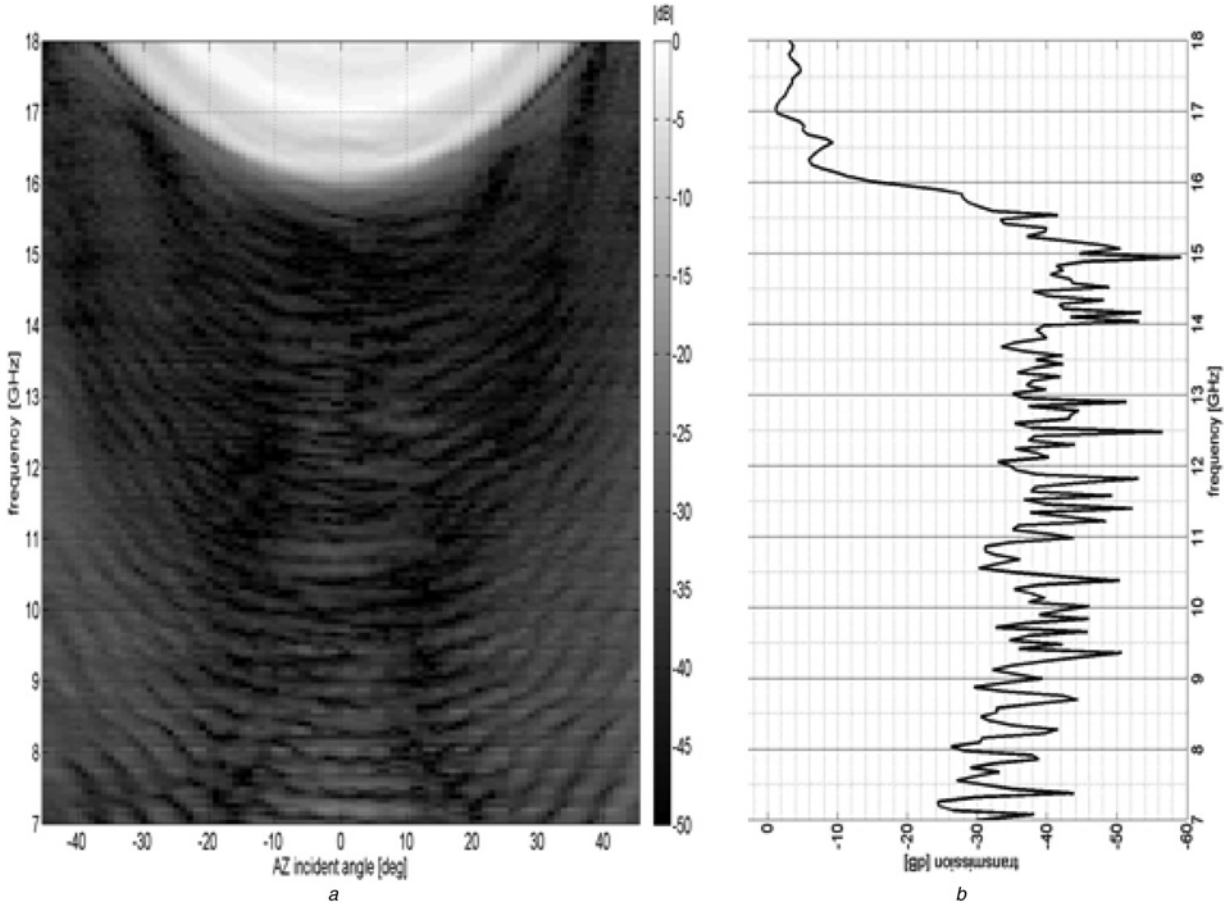


*a* *b*

**Figure 12** *Two-dimensional plot of the measured transmission results for the wire-based MTM structure*

*a* Two-dimensional plot of the measured transmission results against frequency and incident angle in azimuth for the wire-based MTM structure

*b* Transmission against frequency at AZ $= 0^{\circ}$



doi: 10.1049/iet-map.2010.0024

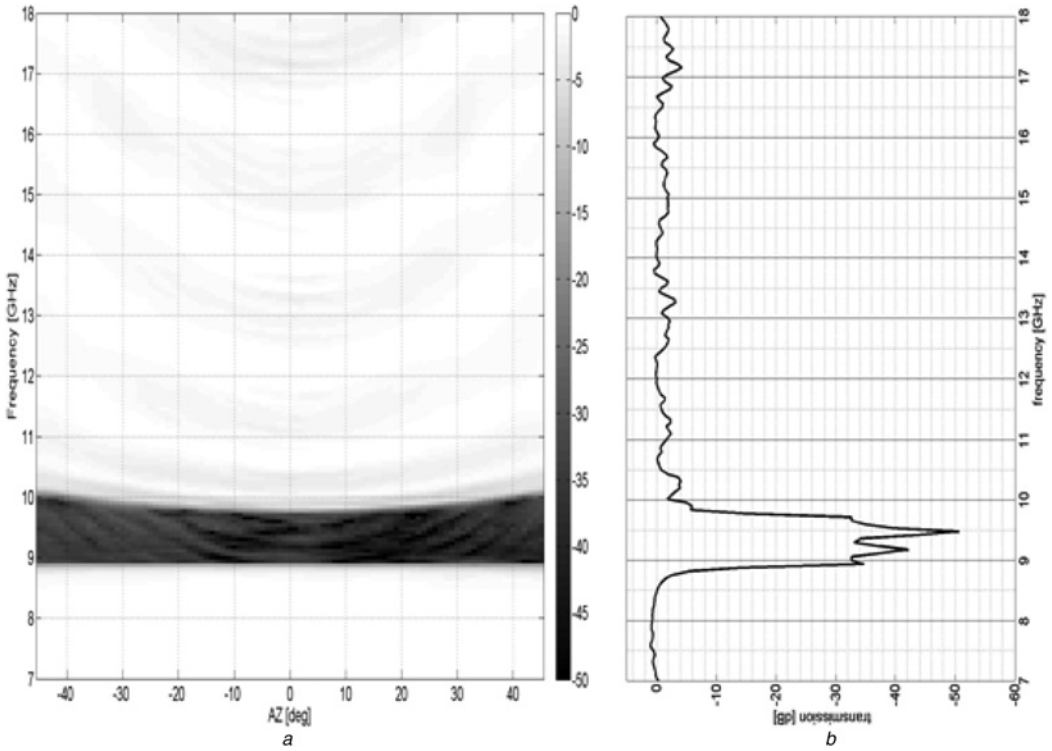


**Figure 13** *Two-dimensional plot of the measured transmission results for the SRR-based MTM structure*

*a* Two-dimensional plot of the measured transmission results against frequency and incident angle in azimuth for the SRR-based MTM structure

*b* Transmission against frequency at AZ = 0°

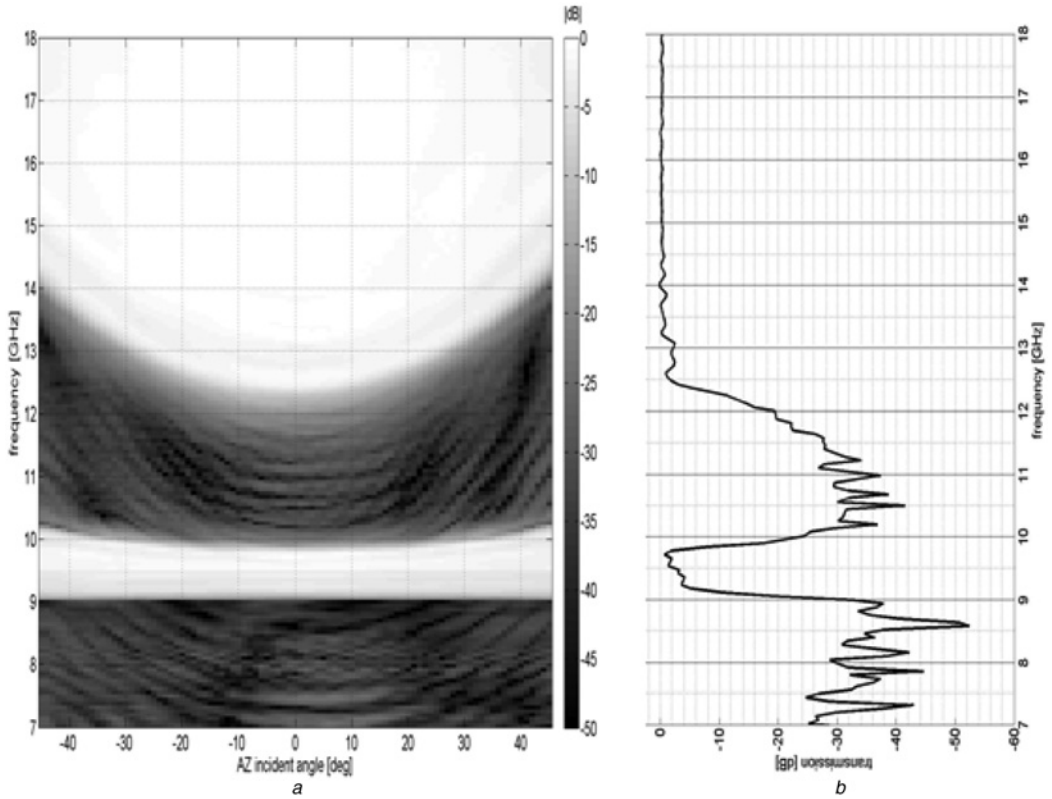


**Figure 14** *Two-dimensional plot of the measured transmission results for the combined wires and SRR-based MTM structure*

*a* Two-dimensional plot of the measured transmission results against frequency and incident angle in azimuth for the combined wires and SRR-based MTM structure

*b* Transmission against frequency at AZ = 0°

Figs. 12–14 show the experimental transmission results of all three prototypes for the entire angular range and for frequencies 7–18 GHz. It can be clearly noticed that for the SNG MTM prototypes (wires or SRRs) there is practically no transmission (average levels of −35 to −45 dB), as expected, in the frequency range 9.15–9.75 GHz, whereas the combined MTM structure experiences very good transmission with a maximum of −0.7 dB at normal incidence. This is the highest value that these authors are aware of that has been reported for experiments with this type of MTM. In addition, it is obvious, based on the simulated and experimental data, that good transmission characteristics are maintained in the incident angular sector of at least $\pm 45^{\circ}$.

## 6 Conclusions

Two independent methods were used for the extraction of the constitutive parameters of large-scale single and DNG MTMs. The large-scale MTMs were used in order to obtain better accuracy and to view the field characteristics within the materials, which cannot be observed in a single unit cell structure. The 'field' extraction method compared inner MTM fields of two types of SNG MTMs to those of an analytic model. The S-parameter method is using the scattering matrices in order to obtain the constitutive parameters from two SNG and one DNG MTMs models. The S-parameter method, originally reported to work unambiguously in thin structures, was improved to enable its use unambiguously for thick structures. Good agreement was obtained between the two methods, thus validating their accuracy. These two methods are fairly easy to implement when designing MTMs, since the available EM simulation tools enable the extraction of the fields within the material as well as its scattering parameters. The DNG nature of the MTM was validated by simulating a lens made entirely of wires and SRRs. The lens had a spherical concave geometry, which refracted the incident waves in the opposite direction to the direction of DPS materials. We also noted a very clear focal point that emerged from this lens at a very close proximity to its expected location based on its extracted permittivity and permeability. All three structures were then etched on a dielectric substrate and measured in an anechoic chamber at frequencies ranging from 7 to 18 GHz and at incident angles ranging from $-45$ to $+45^{\circ}$. The DNG MTM prototype showed a transmission peak of −0.7 dB in its pass band.

## 7 References

[1] VESELAGO V.G.: 'The Electrodynamics of substances with simultaneously negative values of $\varepsilon$ & $\mu$', *Sov. Phys. Usp.*, 1966, **10**, (4), pp. 509–514

[2] PENDRY J.B., HOLDEN A.J., STEWART W.J., YOUNGS I.: 'Extremely low frequency plasmons in metallic mesostructures', *Phys. Rev. Lett.*, 1996, **76**, (25), pp. 4773–4776

[3] PENDRY J.B., HOLDEN A.J., ROBBINS D.J., STEWART W.J.: 'Magnetism from conductors and enhanced nonlinear phenomena', *IEEE Trans. Microw. Theory Tech.*, 1999, **47**, pp. 2075–2084

[4] SMITH D.R., SCHULTZ S., MARKOS P., SOUKOULIS C.M.: 'Determination of effective permittivity and permeability of metamaterials from reflection and transmission coefficients', *Phys. Rev. B*, 2002, **65**, (195104), pp. 1–5

[5] CHEN X., GRZEGORCZYK T.M., WU B.I., PACHECO J., KONG J.A.: 'Robust method to retrieve the constitutive effective parameters of metamaterials', *Phys. Rev. E*, 2004, **70**, (016608), pp. 1–7

[6] SMITH D.R., VIER D.C., KOSCHNY T., SOUKOULIS C.M.: 'Electromagnetic parameter retrieval from inhomogeneous metamaterials', *Phys. Rev. E*, 2005, **71**, (036617), pp. 1–11

[7] ZHOU J., KOSCHNY T., KAFESAKI M., SOUKOULIS C.M.: 'Size dependence and convergence of the retrieval parameters of metamaterials', *Photon Nanostruct. Fundam. Appl.*, 2006, **6**, pp. 96–101

[8] KOSCHNY T., MARKOS P., ECONOMOU E.N., SMITH D.R., VIER D.C., SOUKOULIS C.M.: 'Impact of the inherent periodic structure on the effective medium description of left-handed and related metamaterials', *Phys. Rev. B*, 2005, **71**, (245105), pp. 1–22

[9] AYDIN K., LI Z., SAHIN L., OZBAY E.: 'Negative phase advance in polarization independent, multi-layer negative-index metamaterial', *Opt. Express*, 2008, **16**, (12), pp. 8835–8844

[10] OZBAY E., AYDIN K., CUBUCKU E., BAYINDIR M.: 'Transmission and reflection properties of composite double negative metamaterials in free space', *IEEE Trans. Antennas Propag.*, 2003, **51**, (10), pp. 2592–2595

[11] JORDAN E.C., BALMAIN K.G.: 'Electromagnetic waves and radiating systems' (Prentice-Hall, New Jersey, 1968, 2nd edn.), ch. 5

[12] HOLLANDER Y., SHAVIT R.: 'Constitutive parameter extraction for single & double negative metamaterials and validation of negative refraction'. IEEE Int. Symp. on Antennas and Propagation, Honolulu, Hawaii, June 2007, pp. 2586–2589

[13] JENKINS F.A., WHITE H.E.: 'Fundamentals of optics' (McGraw-Hill, New York, 1957, 3rd edn.), ch. 1




doi: 10.1049/iet-map.2010.0024